JCTC Journal of Chemical Theory and Computation

Article

pubs.acs.org/JCTC

Coarse-Graining the Liquid−Liquid Interfaces with the MARTINI Force Field: How Is the Interfacial Tension Reproduced?

Makha Ndao,[†] Julien Devémy,[†] Aziz Ghoufi,[‡] and Patrice Malfreyt*[,†]

[†]Université Clermont Auvergne, Université Blaise Pascal, Institut de Chimie de Clermont-Ferrand, BP 10448, F-63000 Clermont-Ferrand, France

[‡]Institut de Physique de Rennes, Université Rennes 1, 35042 Rennes, France

ABSTRACT: We report two-phase coarse-grained (CG) simulations of organic−water liquid−liquid interfaces with the MARTINI force field. We discuss the ability of the CG force field to predict quantitatively the interfacial tension of alkanes−water, benzene−water, chloroform−water, and alcohol−water systems. The performance of the prediction of the interfacial tension is evaluated through its dependence on temperature and alkane length. This study contributes to the challenging discussion about the robustness and the transferability of the MARTINI force field to interfacial properties. We have also used the distributions of the molecules along the direction normal to the interface to investigate the composition of the interfacial region and to compare the simulated densities of the coexisting phases with experiments.

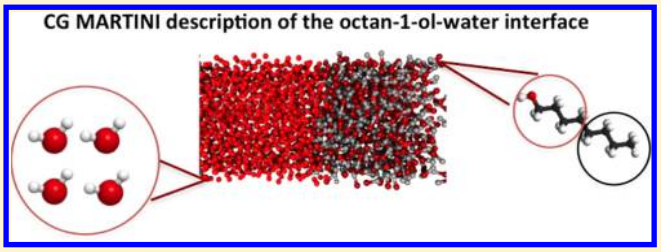

1. INTRODUCTION

Coarse-grained (CG) simulations have gained attention during this past decade to capture the properties of soft matter systems (vesicle formation, membrane−protein assemblies, polymers, formation of micelles). Whereas the key element for the atomistic force field is the atom or the united atom, the CG force field uses a CG particle, often called a bead, that may represent several atoms or molecules, depending on the degree of coarse-gaining used. This simplification allows us to reach larger time and length scales than those accessible by molecular simulations. One possible issue resulting from this reduction of degrees of freedom is the loss of the chemical nature of the molecule.

The top-down and bottom-up parametrization schemes represent then two different alternatives to develop these CG models. Top-down approaches derive parameters from macroscopic properties (compressibility, diffusion)[1−3] and require the use of a well-developed experimental database. Bottom-up approaches use the configurations at the atomistic level to develop interaction forces and parameters for the mesoscopic model.[4−12] The development of a CG force field addresses a number of fundamental issues concerning the choice of the degree of coarse-graining, the way of building of the CG potentials, and the dynamic rescaling imposed by the reduction of the degrees of freedom inside the bead. Nevertheless, this type of methodology has been successfully applied to a variety of polymer melts.[4,8,11,13−16] These CG models have been implemented either in Molecular Dynamics (MD)[4,13−15,17] or in Dissipative Particle Dynamics (DPD)[2,3,16,18−23] simulations.

An other type of CG model is the MARTINI force field,[24−30] which is based mainly on a four-to-one mapping. It means that four heavy atoms plus associated hydrogen atoms are represented by a single bead. For example, the CG water MARTINI model corresponds to four water molecules. Smaller resolution can be applied to ions where a single bead represents the ion with its first hydration shell. A higher resolution (a two-to-one mapping) is often used to model ringlike molecules. The relatively small level of coarse-graining used by the MARTINI force field allows us to model the dispersion and overlap interactions with the 12-6 Lennard-Jones potential. The MARTINI force field has been designed to simulate a broader range of applications without the need to reparameterize the model each time. This was achieved by extensive calibrations of the CG beads against thermodynamic properties. The bonded interactions are then developed from a bottom-up approach by using the atomistic simulations (with force fields based on either the all-atom or united atom descriptions), whereas the parameters of the intermolecular interactions are calibrated from a top-down approach by using the thermodynamic properties of bulk liquids and mixtures (density, free energy of hydration, free energy of vaporization, and partitioning free energies between water and a number of organic phases).

Currently, there is an increasing need to understand what happens at the interfacial region between two liquid phases in terms of specific arrangements and energy. In addition, for more complex interfacial systems involving the presence of amphiphilic molecules, the molecular simulations should become an important tool to rationalize the efficiency of the surfactant at the interface, the tendency to form micellar aggregates, and the impact of the chemical structure on lowering the interfacial tension. The computer simulations

Received: February 15, 2015
Published: July 7, 2015

DOI: 10.1021/acs.jctc.5b00149
J. Chem. Theory Comput. 2015, 11, 3818−3828

Table 1. Lennard-Jones Parameters and Electrostatic Charges for Different Molecules Described through the MARTINI Force Field

CG bead	AA	σ (nm)	ϵ (kJ mol^{-1})	q (e)
	Water			
W	4 H_2O	0.47	4.0	0
WP		0	0	0.46
WM		0	0	−0.46
distance W−WP, W−WM (nm)	0.14			
angle WP−W−WM (rad)	θ_0 = 0, k_θ = 4.2 kJ mol^{-1} rad^{-2}			
	n-Alkane			
C1	C−C−C−C	0.47	3.5	0
distance C1−C1 (nm)	r_0 = 0.47, k_b = 1250 kJ mol^{-1} nm^{-2}			
bending C1−C1−C1	θ_0 = 180°, k_θ = 25 kJ mol^{-1}			
	Cyclohexane			
SC1	C−C	0.43	2.625	0
distance SC1−SC1 (nm)	r_0 = 0.3, k_b = 5000 kJ mol^{-1} nm^{-2}			
	Benzene			
SC5	C═C	0.43	2.625	0
distance SC5−SC5 (nm)	r_0 = 0.27, k_b = 5000 kJ mol^{-1} nm^{-2}			
	Octan-1-ol			
C1	C−C−C−C	0.47	3.5	0
P1	C−C−C−O	0.47	4.5	0
distance C1−P1 (nm)	r_0 = 0.47, k_b = 1250 kJ mol^{-1} nm^{-2}			
	Chloroform			
C4	$CHCl_3$	0.47	3.5	0
	Matrix of Crossed Interactions			
site	site	σ (nm)	ϵ (kJ mol^{-1})	
C1	W	0.47	1.9	
C4	W	0.47	2.565	
SC1	W	0.47	1.9	
SC5	W	0.47	2.945	
P1	W	0.47	4.275	
C1	P1	0.47	2.7	

based upon an atomistic description cannot reach the time scale to observe diffusion to the interface and formation of micelles. By coarse-graining the interactions between atoms, it is then possible to access longer time and length scales. Before tackling multicomponent mixtures, we propose here to apply the MARTINI force field to liquid−liquid interfaces for which the use of atomistic model remains problematic due to the large number of molecules and equilibration time required to model well-developed interfaces. The CG description of these interfaces represents, then, an interesting alternative that merits investigation. Such simulations will test the transferability of the MARTINI model to the interfacial tension. We are faced with two key challenges for the CG MARTINI model: robustness and transferability.

There were, however, some attempts to calculate the interfacial tension of the liquid−vapor interface of water[25] and dodecane[25] by coarse-graining the interactions. Concerning the interfacial tension of water, the different MARTINI water models[25,28] underestimate significantly the interfacial tension, with deviations from experiments ranging from 40% to 60%. The prediction is excellent in the case of the liquid−vapor interface of the dodecane. For the liquid−liquid dodecane−water system, the first simulations carried out with the nonpolarizable version of the water model[25] show a qualitative reproduction of the interfacial tension at 298 K.

In this paper, we propose to apply the MARTINI model to simulate different organic−water liquid−liquid interfaces. We take the route of starting the study by considering an organic phase formed by nonpolar alkanes (linear and cyclic). The alkane molecule is the best candidate to investigate the ability of the force field to predict the interfacial tension for two reasons. First, the alkane molecule is formed by only one type of CG particle. Second, both organic and water phases are relatively well-separated, avoiding the need to consider here the impact of the degree of coarse-graining on the results. We present the results of the interfacial tension and illustrate its dependence with respect to temperature and alkane chain length. We extend this study to the benzene−water liquid−liquid interface that presents an interfacial tension significantly lower than that of the cyclohexane−water system. We increase the polarity of the organic phase by investigating the chloroform−water liquid−liquid system. Is the degree of coarse-graining of chloroform able to describe what happens at the interface? Does this CG description impact the interfacial tension? We complete this study by modeling an interface formed by octan-1-ol and water molecules for which the

DOI: 10.1021/acs.jctc.5b00149
J. Chem. Theory Comput. 2015, 11, 3818−3828

interactions are stronger and lead to specific orientations. Is the CG MARTINI description able to consider specific local structural properties? Let us recall that the development of new parameters for the MARTINI force field is outside the scope of this study. As a result, we take the route of using the latest version of the MARTINI force field with the polarizable version of the water model.

The paper is organized as follows. Section 2 describes the MARTINI model by focusing on the shifted Lennard-Jones and electrostatic potentials. The CG description of each molecule is given with the corresponding parameters. This section also presents the different approaches for the calculation of the interfacial tension. Section 3 contains the discussions from methodological and quantitative viewpoints. Section 4 concludes on this work.

2. SIMULATION DETAILS

2.1. Potential Models. The MARTINI force field[24−29] considers interaction sites called beads or coarse-grained (CG) particles. On average, one bead contains four heavy atoms, but a different degree of coarse-graining is applied to ring structures and ions. The total energy U_{tot} sums the nonbonded energy U_{nb} and the bonded energy U_b.

2.1.1. Nonbonded Interactions. Let us consider a simulation box formed by a total number of N molecules, where n_i and n_j are the numbers of force centers in the molecules i and j, respectively. In the case of the intermolecular interactions, the nonbonded interactions U_{nb} of eq 1 occur between particle a and particle b of molecules i and j, respectively. These nonbonded interactions are then calculated using

$$U_{nb} = \sum_{i=1}^{N-1} \sum_{j>i}^{N} \sum_{a=1}^{n_i} \sum_{b=1}^{n_j} U_{LJS}(r_{iajb}) + U_{ELS}(r_{iajb}) \tag{1}$$

where the dispersion−repulsion (U_{LJS}) and electrostatic (U_{ELS}) interactions are modeled by shifted potentials. In eq 1, r_{iajb} is the distance between force center of particle a in molecule i and force center of particle b in molecule j.

In the case of intramolecular interactions, the nonobonded interactions are calculated between beads separated by more of two bonds by using the same shifted Lennard-Jones (U_{LJS}) and Coulombic (U_{ELS}) potentials.

The dispersion−repulsion interactions are then represented by the Lennard-Jones potential (U_{LJS}) modified by a cubic spline function so that the potential and force are continuous and smoothly shifted to zero between the cutoff radii r_s and r_c.

$$U_{LJS}(r_{iajb}) = \begin{cases} U_{LJ}(r_{iajb}) - U_{LJ}(r_c) - C & r_{iajb} < r_s \\ U_{LJ}(r_{iajb}) - U_{LJ}(r_c) - f(r_{iajb}, r_s, r_c) - C & r_s \le r_{iajb} < r_c \\ 0 & r_{iajb} \ge r_c \end{cases} \tag{2}$$

where the Lennard-Jones potential $U_{LJ}(r_{iajb})$ is given by the following expression:

$$U_{LJ}(r_{iajb}) = 4\epsilon_{ab}\left[\left(\frac{\sigma_{ab}}{r_{iajb}}\right)^{12} - \left(\frac{\sigma_{ab}}{r_{iajb}}\right)^{6}\right] \tag{3}$$

ϵ_{ab} is the energy parameter of the interaction, and σ_{ab} is the Lennard-Jones core diameter. The functions $f(r_{iajb}, r_s, r_c)$ and the constant C are given in Appendix A for the Lennard-Jones function. The values of ϵ_{aa} for identical CG beads and ϵ_{ab} for unlike CG beads are given in Table 1 for completeness.

The electrostatic interactions are represented by a Coulombic potential (U_{ELS}) which is shifted to zero from r_s = 0 nm to r_c = 1.2 nm. This shift amounts to modeling the effect of a distance-dependent screening. The resulting expression of the shifted Coulombic potential is then

$$U_{ELS}(r_{iajb}) = \begin{cases} U_{COU}(r_{iajb}) - U_{COU}(r_c) - \frac{1}{3}Dr_{iajb}^3 - \frac{1}{4}Er_{iajb}^4 - F & r_{iajb} < r_c \\ 0 & r_{iajb} \ge r_c \end{cases} \tag{4}$$

$U_{COU}(r_{iajb})$ is defined by

$$U_{COU}(r_{iajb}) = \frac{q_{ia}q_{jb}}{4\pi\epsilon_0\epsilon_r r_{iajb}} \tag{5}$$

where q_{ia} is the charge of the particle a in molecule i. ϵ_0 is the permittivity in a vacuum, and ϵ_r is the relative dielectric constant. The constants D, E, and F are given in Appendix B.

2.1.2. Bonded Interactions. In the MARTINI model, the bond between two beads a and b is described by a harmonic potential $U_{bond}(r_{ab})$,

$$U_{bond}(r_{ab}) = \frac{1}{2}k_{bond}(r_{ab} - r_0)^2 \tag{6}$$

where r_{ab} is the distance between two beads a and b and r_0 the equilibrium distance between these two beads. The values of k_{bond} and r_0 are given in Table 1 for the different molecules studied here.

A bending potential represented by a harmonic potential of the cosine is used to model the interaction between three consecutive beads. This potential expresses as

$$U_{bend}(\theta) = \frac{1}{2}k_{bend}(\cos(\theta) - \cos(\theta_0))^2 \tag{7}$$

The values of k_{bend} and θ_0 are listed in Table 1.

2.1.3. Coarse-Grained Description of the Molecules. The polarizable water model of the MARTINI force field[28] considers three particles, W, WP, and WM, along with five parameters. The central W particle is connected to WP and WM particles by constrained bonds of length of 0.14 nm and by a harmonic angle potential function with θ_0 and k_θ parameters. W, WP, and WM have an equal mass of 24 g mol^{-1}. The values of the parameters for water are given in Table 1. The CG MARTINI water model represents four water molecules. The reader is redirected to ref 28 for a comprehensive description of the model. Because all the simulations use the polarizable version of the water MARTINI model, ϵ_r is taken equal to 2.5. This water model has been developed from simulations using the short-range functions of eqs 2 and 4. Reference 28 also concludes that the polarizable MARTINI water model can be used with the PME method[31] and the Coulombic potential with no effect on the results.

For the linear alkanes,[24] *n*-octane is modeled by using two beads, *n*-dodecane by three beads, and *n*-dodecane by four beads as illustrated in Table 1 and Figure 1. It means that each bead (C_1) of the linear alkane molecule has a mass of 72 g mol^{-1}. For the cyclohexane (SC_1) and benzene (SC_5) molecules,[32] we use three beads in a triangular ring configuration (see Figure 1). The mass of the beads in these ring structures is then equal to 45 g mol^{-1}. The σ parameter is

DOI: 10.1021/acs.jctc.5b00149
J. Chem. Theory Comput. 2015, 11, 3818−3828

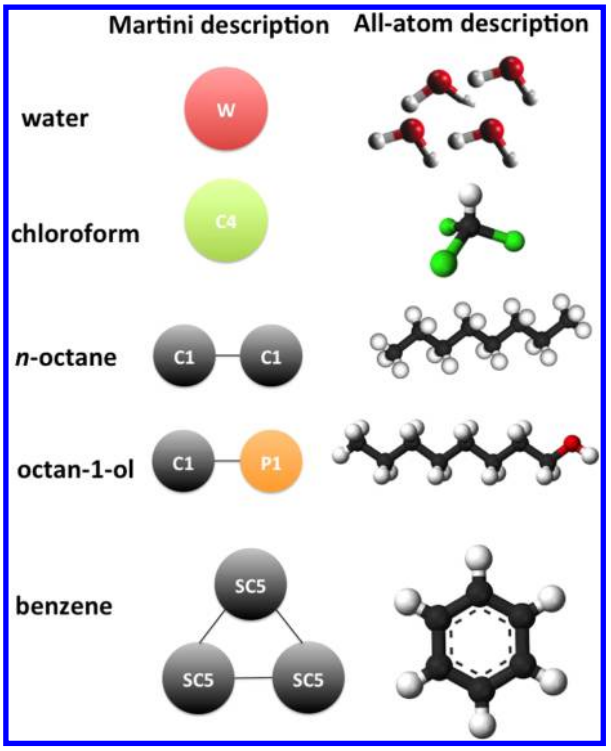

Figure 1. Illustration of the CG descriptions in the MARTINI force field with the different types of CG beads along with the atomistic representations of the molecules.

set to 0.43 nm rather than 0.47 nm, and the value of ϵ is scaled to 75% of the original value of C_1 (see Table 1). The octanol molecule is modeled by two different beads, C_1 and P_1, whose parameters are given in Table 1, whereas the chloroform is described by one bead, C_4. The mass of these beads, C_1, P_1, and C_4, is fixed to 72 g mol^{-1}.

2.2. Interfacial Tension. We take the route of calculating the interfacial tension by using three different operational expressions that allow to calculate the profile of the interfacial tension along the normal to the liquid−liquid interface. The profile is a key element to check the stability of the CG two-phase simulations. The long-range corrections to the interfacial tension are equal to zero since the potentials used for the dispersion−repulsion and electrostatic interactions are shifted to zero at the cutoff radius. The method of Irving and Kirkwood (IK)[33] expresses the interfacial tension from the local components of the pressure tensor as

$$\gamma_{IK} = \int_{-L_z/2}^{L_z/2} (p_N(z_k) - p_T(z_k))\, dz_k \tag{8}$$

where $p_N(z_k)$ and $p_T(z_k)$ are the normal and tangential components of the pressure tensor along the normal to the surface, respectively. The IK method is described thoroughly in previous papers.[34−37]

The test-area (TA) method[38] is based upon a thermodynamic route and expresses the interfacial tension as a change in the free energy for an infinitesimal change in the surface area. The operational expression for the calculation of γ within the TA method is

$$\gamma_{TA} = \sum_k \lim_{\xi \to 0} -\frac{k_B T}{\Delta A} \ln \left\langle \exp\left(-\frac{(U^{(A+\Delta A)}(z_k, \mathbf{r}'^N) - U^{(A)}(z_k, \mathbf{r}^N))}{k_B T} \right) \right\rangle_{k,A} \tag{9}$$

$\langle \cdots \rangle_{k,A}$ indicates that the average is carried out over the reference state and the k slabs. $U^{(A+\Delta A)}(z_k,\mathbf{r}'^N)$ and $U^{(A)}(z_k,\mathbf{r}^N)$ are the configurational energies of the slab k in the perturbed and reference states. The reader is directed to ref 37 for a description of the operational expression of the local energy. Thermodynamic consistency requires that the surface tension in the direct and reverse directions must be equal in magnitude and in opposite sign: the calculation in the direct direction involves an increase of the surface area $(A + \Delta A)$, whereas a decrease of the surface area $(A - \Delta A)$ is involved in the reverse path. This is satisfied when the configuration space of the perturbed system matches that of the reference system. This requirement implies the use of an appropriate value of ξ. The value of ξ must satisfy two constraints: this value should be small to allow an accurate calculation of the interfacial tension from eq 9 and large enough to provide reasonable statistics for the Boltzmann factor. We find that $\xi = 1.0 \times 10^{-7}$ represents the best compromise to obtain a good profile of the interfacial tension and an agreement between the direct and inverse values of γ_{TA}. For completeness, ξ was taken to be 1.0×10^{-4} for the calculation of γ_{TA} in simulations with atomistic force fields.[37]

The third method (KBZ), based upon the KB expression, uses the derivative of the potential with respect to the surface, as described by the following equation:

$$\gamma_{KBZ} = \left\langle \frac{\partial U}{\partial A} \right\rangle_0 = \sum_k^{N_s} \left\langle \frac{\partial U_{z_k}}{\partial A} \right\rangle_0 = \sum_k^{N_s} \gamma_{KBZ}(z_k) = \sum_k^{N_s} (\gamma_{KBZ}^{LJS}(z_k) + \gamma_{KBZ}^{ELS}(z_k)) \tag{10}$$

The reader is redirected to the original paper by Ghoufi et al.[39]

2.3. Molecular Dynamics Simulations. The simulation box was a rectangular parallelepipedic box of dimensions L_x L_y L_z (L_x = L_y = 5.4 nm) with water and different organic molecules. Initially, homogeneous boxes of water and organic molecules were simulated in the NVT ensemble in order to equilibrate the two boxes at the target temperature. We used the Packmol package[40] to build the initial CG configurations. These two boxes have the same L_x (5.4 nm) and L_y (5.4 nm) dimensions. A new box is obtained by replicating along the z-axis the box of the organic phase and the water box. The periodic boundary conditions can then be applied in the three directions. This resulting box was equilibrated in the NVT ensemble in order to relax the system. The total number of water beads was 2863, and the number of organic molecules was fixed to 1186. The MD simulations were performed with a modified version of the DL_POLY code.[41,42] The changes consist of implementing the shifting of the forces from r_s to r_c and the Np_NAT statistical ensemble. Indeed, the simulations were performed in the Np_NAT ensemble by using the Berendsen[43] algorithm, where A represents the interfacial area. The normal component of the pressure tensor p_N was fixed to 0.1 MPa and T = 298 K. The volume of the system was changed by varying the longitudinal dimension L_z of the box

DOI: 10.1021/acs.jctc.5b00149
J. Chem. Theory Comput. 2015, 11, 3818−3828

while keeping the interfacial area A constant. Because the longitudinal dimension of the box changes during the course of the simulation, the profiles along the direction normal to the surface will be plotted as a function of the reduced property z^* defined by z_k/L_z. The equation of motions were solved using a time step of 30 fs.[24,25,32] In the next section, we discuss the results of interfacial tension with respect to different time steps (10 and 20 fs). The equilibration period was carried out over 5 $\times$ 10^5 time steps and the production phase over 1.0 $\times$ 10^7 time steps. It means that the CG simulations reported here on the liquid−liquid interfaces are carried out 0.3 μs. Standard deviations of the ensemble averages were calculating by breaking the production runs into block averages. The calculated number of block averages was adjusted in order to allow the convergence of the interfacial tension within each block. The cutoff radius r_c was set to 1.2 nm and r_s = 0.9 nm in line with the cutoff radii used for the development of the MARTINI force field. Figure 2 focuses on the interfacial region of two systems.

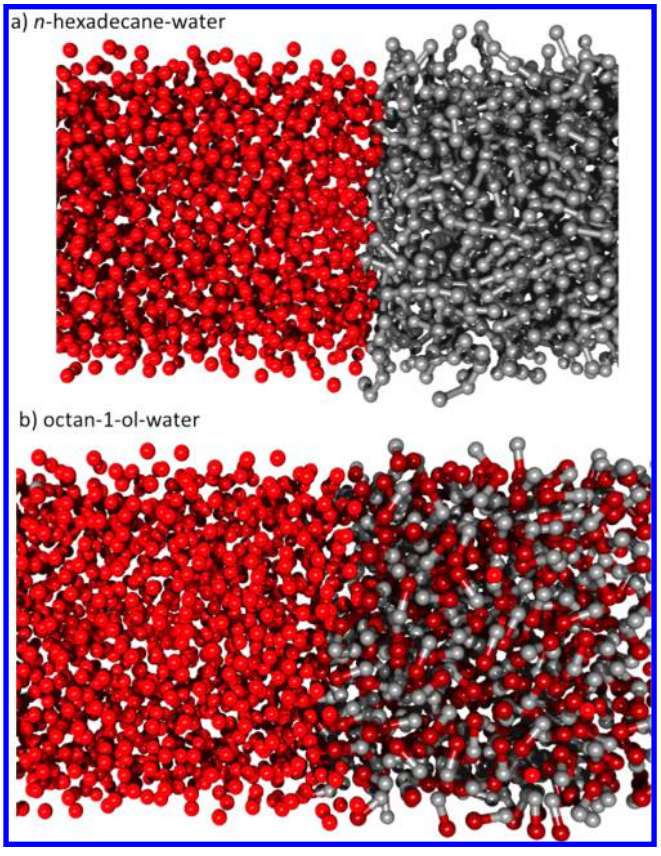

Figure 2. Interfacial region of two different organic−water liquid−liquid systems as indicated in the legend at 300 K and 0.1 MPa. Water bead (W, red), *n*-hexadecane bead (C1, gray), and 1-octanol bead (C1, gray; P1, red).

3. RESULTS AND DISCUSSIONS

3.1. Methodological Aspect. Let us begin this section with a methodological discussion about the calculation of the interfacial tension of liquid−liquid configurations. This is an essential step to check the validity of the two-phase CG simulations through the calculation of the profiles of the interfacial tension along the direction normal to the interface. First, Figure 3a shows the trajectory of the interfacial tension of

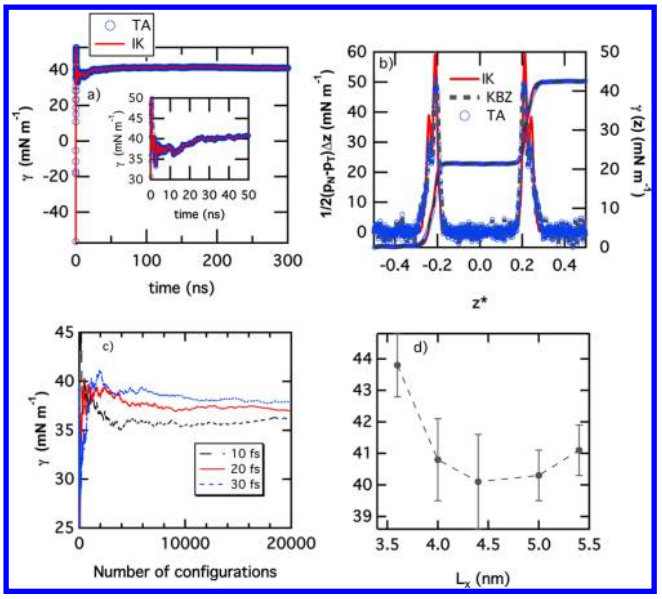

Figure 3. (a) Interfacial tension calculated using the two approaches, TA and IK, as a function of time for the *n*-octane−water interface at 323 K and 0.1 MPa. The inset focuses on the first 50 ns. (b) Profiles of the difference $p_N - p_T$ components of the pressure tensor (left axis) and of its integral (right axis) for the *n*-dodecane−water system. (c) Interfacial tension of the *n*-octane−water interface at 323 K as a function of the number of configurations for three time steps. (d) Interfacial tension of the *n*-octane−water interface at 300 K for different lengths L_x.

the *n*-octane−water liquid−liquid interface calculated by using the TA and IK definitions at 300 K and 0.1 MPa. The average interfacial tension converges very well over 300 ns: the values are equal to 41.09, 41.07, and 41.08 mN m^{-1} for the IK, TA, and KBZ approaches, respectively. Considering that the statistical fluctuations of the interfacial tension calculated by using block averages are in the order of 0.8 mN m^{-1}, all the definitions lead to the same value of the interfacial tension, i.e., 41.1 $\pm$ 0.8 mN m^{-1}. The inset focuses on the first 50 ns and establishes a convergence of the interfacial property after 30 ns. It shows the possibility to decompose the trajectory over 300 ns into different blocks averages to calculate the fluctuations of the interfacial tension. This time-dependence of the interfacial tension explains why we obtain an interfacial tension of the octane−water system (T = 300 K) slightly different to that obtained in a previous simulation[37] carried out over a period of only 10 ns. In our previous work,[37] we observed differences between the TA, IK, and KBZ techniques. These differences are explained by the calculation of the electrostatic energy which was based on the calculation of the separation distance between the centers-of-mass of molecules i and j ($r_{ij} < r_c$) for the selection of molecules that contribute to the energy. Here, we replace the center-of-mass distance between two molecules by the distance between beads a and b of each molecule ($r_{iajb} < r_c$), indicating that a molecule can partially contribute to the intermolecular electrostatic energy. This change makes the IK and TA approaches perfectly identical, as shown in Table 2. Let us recall that the TA method is based upon the calculation of the energy and the IK method on the calculation of the forces. This subtlety leads to differences between the intrinsic part (with no long-range corrections added) of the interfacial tension calculated with IK and TA when truncated potentials are used. For truncated and shifted forces and potentials that

DOI: 10.1021/acs.jctc.5b00149
J. Chem. Theory Comput. 2015, 11, 3818−3828

Table 2. Interfacial Tensions (mN m^{-1}) of Different Liquid−Liquid Interfaces Calculated by the IK, TA, and KBZ Definitions[a]

T (K)	γ_{IK}	γ_{KBZ}	γ_{TA}	$\langle\gamma\rangle$	γ_{exp}
		n-Octane−Water			
300	41.1_8	41.1_8	41.1_8	41.1_8	51.2
308	39.5_7	39.5_7	39.5_7	39.5_8	50.2
318	38.4_3	38.4_3	38.4_3	38.4_3	49.4
323	37.9_9	37.9_9	37.9_9	37.9_9	48.9
		n-Dodecane−Water			
300	42.6_{10}	42.6_{10}	42.6_{10}	42.6_{10}	52.8
		n-Hexadecane−Water			
300	43.2_{10}	43.2_{10}	43.2_{10}	43.2_{10}	53.3
		Cyclohexane−Water			
300	43.5_{13}	43.5_{12}	43.5_{12}	43.5_{12}	47.9
323	41.2_6	41.2_6	41.2_6	41.2_6	43.9
343	38.5_{12}	38.5_{12}	38.5_{12}	38.5_{12}	40.7
		Benzene−Water			
300	10.5_9	10.5_8	10.5_8	10.5_8	32.5
323	9.4_7	9.4_7	9.4_7	9.4_7	29.0
343	6.6_6	6.6_6	6.6_6	6.6_6	26.3
		Chloroform−Water			
300	24.0_5	24.0_5	24.0_5	24.0_5	31.6
		Octan-1-ol−Water			
300	19.7_7	19.7_7	19.7_7	19.7_7	8.5

[a]The experimental interfacial tensions, given for comparison, are taken from ref 50 for the linear-alkane−water systems, from ref 49 for the cyclohexane−water and benzene−water systems, and from ref 51 for the chlorofom−water and octanol−water systems. The subscripts give the accuracy of the last decimal(s), e.g., 41.1_8 means 41.1 ± 0.8.

remain continuous at the cutoff radius, we should not expect any differences between these two techniques. This is exactly what we observe here in line with previous simulations using cubic spline functions.[44]

Second, Figure 3b shows the profiles of the local interfacial tension γ (z^*) as a function of the reduced position ($z^* = z/L_z$) for the *n*-dodecane−water system at 300 K. Since the profiles calculated by using the IK approach are the most widespread in the field of the two-phase simulations, we compare it with those calculated with TA and KBZ recently developed. The profiles show contributions in the bulk liquid phases that oscillates around zero and two positive peaks in the interfacial regions. These two peaks are well-defined and symmetric, indicating that the two-phase simulations provide two well-equilibrated liquid−liquid interfaces. In addition, the profile γ (z^*) shows that the two interfacial regions contribute in the same way to the interfacial tension with two symmetric peaks. The fact that the integral is constant in the bulk liquid regions means that the liquid phases do not contribute to the interfacial tension and indicates that the liquid regions are well-developed. Consequently, the two interfacial regions are independent, with no interaction between them. The little difference between the three definitions is found in a more marked peak in the interfacial region with the IK approach. This slight difference in the magnitude of the interfacial peak does not impact on the total interfacial tension. Interestingly, all the definitions exhibit a shoulder in the peaks toward the organic phase. The presence of this shoulder in these interfacial regions has already been discussed in previous papers.[37,45] The interfacial tensions calculated using these three definitions are then reported in Table 2. The values can be considered as identical (with one digit after the decimal point) for IK, TA, and KBZ.

Panel c of Figure 3 shows the interfacial tension of the *n*-octane−water system as a function of the saved configurations for three time steps (τ = 10, 20, and 30 fs) at T = 323 K. Each configuration is saved at every 100 steps, and the number of steps of the acquisition phase is 2×10^6 steps. The effective simulation time for these time steps is then 20, 40, and 60 ns. Independently of the value of τ, we observe the convergence of the interfacial tension. The average interfacial tension is then 36.1 ± 0.7, 37.0 ± 1.1, and 37.8 ± 1.0 mN m^{-1} for time steps τ = 10, 20, and 30 fs, respectively. For this range of time steps, we do not observe any significant dependence of the surface on this parameter within the statistical fluctuations. We can conclude that a larger time (30 fs) step requires a longer simulation time (60 ns) for the convergence of the interfacial tension. When τ increases from 10 to 30 fs, we observe an increasing deviation between the average and target temperatures (from 1% to 5%). The reader is directed to refs 46−48 for a comprehensive study on the impact of the time step on the simulated properties.

Another methodological aspect that may impact the results of interfacial tension is the dependence of this property on system sizes. Figure 3d shows the dependence of the interfacial tension of the interfacial area defined by ($A = L_xL_y$). From L_x = 4.0 nm, the variations of the interfacial tension with respect to the box size is within the statistical fluctuations. However, size effects occurring at smaller box sizes must be further investigated in a next study. From this methodological part, we may conclude that the computational procedure (time step, system size, calculation of the interfacial tension) is consistent with an accurate calculation of the interfacial tension. As a result, the deviations between simulated and experimental interfacial tensions cannot be explained by methodological aspects.

3.2. Prediction of the Interfacial Tension. We turn now attention to the ability of the coarse-grained MARTINI force field to reproduce quantitatively the interfacial tension of various organic−water liquid−liquid interfaces. Figure 4 reports the correlation between the simulated and experimental

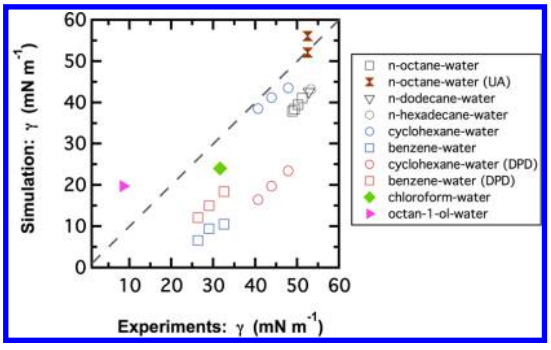

Figure 4. Correlation diagram between the simulated and experimental interfacial tensions for various liquid−liquid interfacial systems. The interfacial tensions calculated from DPD simulations are taken in ref 53.

DOI: 10.1021/acs.jctc.5b00149
J. Chem. Theory Comput. 2015, 11, 3818−3828

interfacial tensions of different organic–water interfaces.[49−51] We add for comparison the interfacial tensions calculated from atomistic models[37,52] and CG models.[53] The values of the interfacial tensions calculated with the CG MARTINI model are listed in Table 2 along with the experimental ones. First, except for the benzene–water system, we observe that the CG MARTINI force field predicts the interfacial tension within 10 mN m^{-1} from experiments. The CG force field underestimates, on the one hand, the interfacial tension of alkane–water and chloroform–water systems by 10 mN m^{-1} but, on the other hand, overestimates that of the alcohol–water binary system by the same deviation. Actually, this deviation represents the quality of the prediction which we may expect from the current version of the MARTINI force field. In some cases, the prediction can perform very well as for example, the cyclohexane–water system. For the benzene–water system, the CG simulation gives very poor estimates of the interfacial tension with deviations that can reach 20 mN m^{-1}.

The CG simulations of the *n*-alkane–water using the MARTINI description reproduce the interfacial tension with a deviation of 20%, which is no so poor compared to simulations with atomistic models[54,55] that show some limitations in the production of well-equilibrated liquid–liquid complex interfacial systems. We have added in Figure 4 the interfacial tensions of the benzene–water and cyclohexane–water systems calculated from CG models[53] used with the DPD method. The prediction of the interfacial tension is slightly better with the CG DPD model for the benzene–water systems whereas the prediction of the interfacial tension of the cyclohexane–water system with the CG DPD model is worse than that obtained with the MARTINI model. Before to investigate the distributions of the molecules along the normal to the surface, we propose now to evaluate how the dependence of the interfacial tension on temperature and alkane length is reproduced.

To do so, we report in part a of Figure 5, the interfacial tension of the *n*-octane–water liquid–liquid interface as a function of the temperature. The relative deviations between experimental and simulated interfacial tensions are on the order of 20% but the experimental decrease of the interfacial with temperature is respected by the two-phase simulations. As a result, Figure 5b shows the variation $\Delta\gamma = \gamma_T - \gamma_{(T=300\ K)}$ of the interfacial tension as a function of the temperature. Whereas the experimental slope of $\gamma = f(T)$ is −0.10 mN m^{-1} K^{-1}, the simulated slope is −0.13 $^{-1}$ K^{-1}, indicating an overestimation of the temperature dependence of the interfacial tension. Interestingly, part c of Figure 5 reports the evolution of the interfacial tension of *n*-alkane–water liquid–liquid interfaces as a function of the alkane length. The simulations reproduce quantitatively the alkane-length dependence of the interfacial tension, indicating a certain transferability of the CG force field in the alkane length for the interfacial tension. When we examine in Figure 6a the temperature dependence of the interfacial tension of the cyclohexane–water and benzene–water interfaces, we observe that the decrease of the interfacial tension with the temperature is reproduced, and a quantitative agreement with the experiments is obtained in the range of temperature for only the cyclohexane–water system whereas the GC DPD simulations show quantitative deviations from the experiments.

Panel b of Figure 6 represents the variations $\Delta\gamma = \gamma_T - \gamma_{(T=300\ K)}$ calculated from the MARTINI force field along with the corresponding experimental and calculated CG DPD

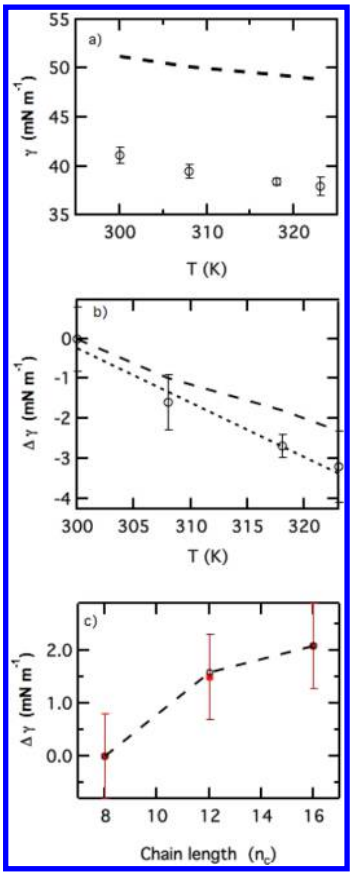

Figure 5. (a) Interfacial tension of the *n*-octane–water liquid–liquid system as a function of the temperature. (b) Relative interfacial tension $\Delta\gamma = \gamma_T - \gamma_{T=300\ K}$ with the fitting curve represented by a dotted line. (c) Relative interfacial tension $\Delta\gamma = \gamma - \gamma_{n_C=8}$ as a function of the alkane length defined in terms of the number of carbons. The dashed lines correspond to the experimental interfacial tensions.[50,51]

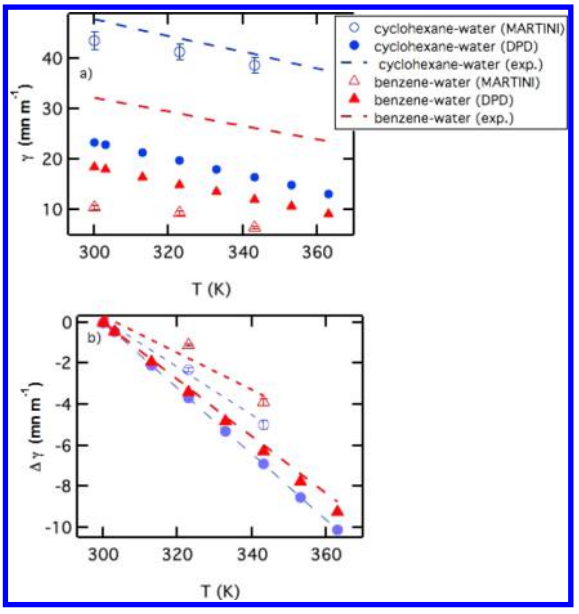

Figure 6. (a) Interfacial tension of the cyclohexane–water and benzene–water liquid–liquid systems as a function of the temperature. (b) Relative interfacial tension $\Delta\gamma = \gamma_T - \gamma_{T=300\ K}$. The experimental values are taken from ref 49, and the simulated interfacial tension from DPD simulations can be found in ref 53.

DOI: 10.1021/acs.jctc.5b00149
J. Chem. Theory Comput. 2015, 11, 3818−3828

interfacial tensions.[53] The temperature dependence of the interfacial tension of the DPD model give slopes of −0.15 and −0.16 mN m^{-1} K^{-1} for the benzene−water and cyclohexane−water systems, respectively. The CG simulations using the MARTINI force field underestimate the slopes with values of −0.09 and −0.11 mN m^{-1} K^{-1} against experimental slopes[49] of −0.14 and −0.16 mN m^{-1} K^{-1} for the benzene−water and cyclohexane−water systems, respectively. However, the MARTINI force field reproduces the difference between the experimental slopes.

We can conclude from the analysis of the interfacial tension of the liquid−liquid interface that the interfacial tension of the *n*-alkanes−water interface is correctly reproduced as well as its dependence on temperature and alkane length. The reproduction of the interfacial tension of the cyclohexane−water is also reasonable. The CG MARTINI force field reproduces the fact that the interfacial tension of the benzene−water system is smaller than that of the cyclohexane−water system but accentuates significantly this difference. We propose now to examine the molecular density profiles along the normal to the interface to check how the coexisting densities are predicted and how the interfacial regions are described in terms of CG units. The analysis of these profiles can help us to understand the impact of the degree of coarse-graining on the description of the interfacial region.

3.3. Molecular Density Profiles. The molecular density profiles of water and *n*-octane molecules are shown in Figure 7a at two different temperatures at 0.1 MPa. The fact to impose the normal pressure constant makes the simulations purely predictive for the coexisting densities. We observe that the density profiles are well-developed and that the values of the water and octane densities decrease with the temperature. At T = 323 K, we find that the water density is 1024 kg m^{-3} (ρ_{exp} = 987 kg m^{-3}) and the octane density is 780 kg m^{-3} (ρ_{exp} = 679 kg m^{-3}), leading to deviations from experiments[51] of about 4% for water and 15% for the alkane (see Table 3). We also find that the density difference between the liquid phases is equal to 244 kg m^{-3} with the MARTINI force field, whereas the experimental corresponding difference[51] is 308 kg m^{-3}. This calculated difference becomes 230 and 220 kg m^{-3} for the *n*-dodecane−water and *n*-hexadecane−water systems (see Table 3), respectively. For these systems, the deviation from experiments is about 10%. For the linear alkanes, the simulated liquid densities are then overestimated whereas the density difference between the two phases are underestimated. For the linear alkanes, the prediction of the coexisting bulk densities and of the temperature dependence of these densities is reasonable. The interface is sharp respecting the picture of two well-separated oil and water phases.

Interestingly, the density profiles of benzene and water molecules are given at two temperatures in part b of Figure 7, and the simulated densities are given in Table 3. The liquid density of the benzene phase in the two-phase system is underestimated by 20% with respect to experiments[56] whereas the MARTINI force field underestimates the liquid density of the cyclohexane phase by only 7% in the cyclohexane−water liquid−liquid system. The inability of the original model[25] to predict the liquid density of the benzene has been already established.[25] We observe however that the MARTINI force field predicts a wider interfacial region compared to that observed with linear alkanes (see Figure 7b), in line with an expected slight decrease of the interfacial tension.

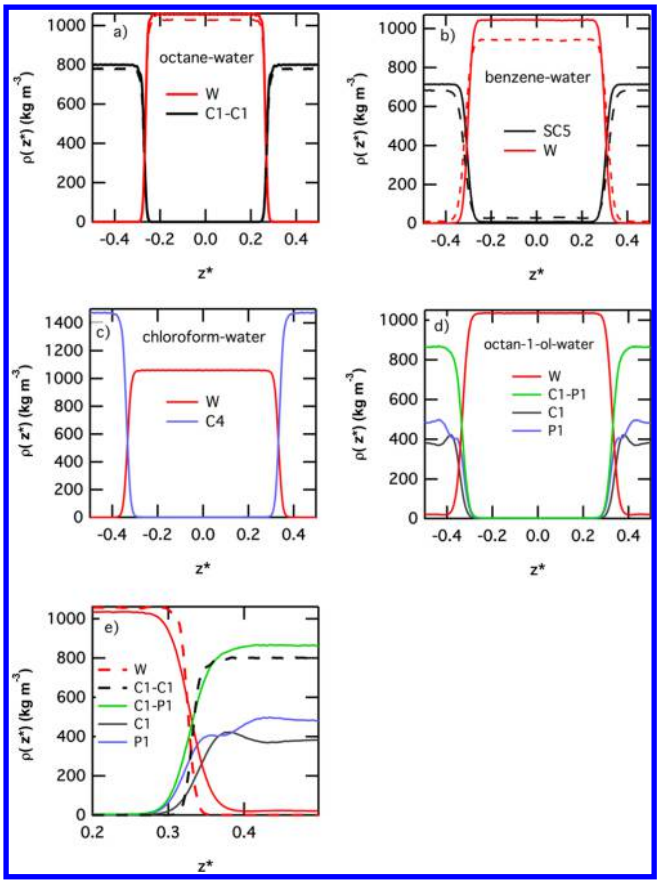

Figure 7. Molecular density profiles of different organic−water interfacial systems. The solid and dashed lines in panels a and b correspond to the density profiles calculated at T = 300 K and T = 323 K, respectively. Panels c and d show the molecular density profiles of the chloroform−water and octan-1-ol−water systems, respectively. Panel e shows the molecular density profiles of the *n*-octane−water (dashed lines) and octan-1-ol−water (solid lines) systems.

Figure 7c shows the density profiles of the chloroform and water molecules in the two-phase system. The density of the organic phase is very well-reproduced with a density of about 1476 kg m^{-3} (see Table 3) leading to a deviation of less than 1% whereas the water density is 1062 kg m^{-3}. The bad quality of the reproduction of the interfacial tension is explained by the degree of coarse-graining of the chloroform that does not impact however on the bulk properties.[56] Nevertheless, at the chloroform−water interface,[57,58] it is well-known that the increase of polarity of the chloroform with respect to alkanes modifies the degree of water structuring at the interface and explains why the interface tension of the chloroform−water system is smaller to that of the alkane−water systems. In addition, in the interfacial region, there is a creation of an electric field that tends to orient the chloroform molecules with the hydrogen atoms pointing toward the water phase. This specificity cannot be captured by this CG description. Only a compensation through a top-down approach could improve the value of the interfacial tension of the chloroform−water system.

We now turn our attention to the octan-1-ol−water liquid−liquid system. Table 3 shows simulated densities of the water and alcohol phases that deviate by less than 5% and a relative density between the alcohol and water phases in agreement with the corresponding experimental value. We complete this analysis by plotting the density profiles in Figure 7d,e. In the

DOI: 10.1021/acs.jctc.5b00149
J. Chem. Theory Comput. 2015, 11, 3818−3828

Table 3. Densities (kg m^{-3}) of the Organic and Water Phases Calculated from CG Simulations Using the MARTINI Force Field[a]

T (K)	$\rho^{CG}_{organic}$	$\rho^{exp}_{organic}$	ρ^{CG}_{water}	ρ^{exp}_{water}
		n-Octane−Water		
300	799	700	1052	997
308	791	688	1046	990
318	785		1035	989
323	780	679	1024	987
		n-Dodecane−Water		
300	822	750	1052	997
		n-Hexadecane−Water		
300	832	770	1052	997
		Cyclohexane−Water		
300	721	778	1052	997
323	704		1022	987
343	693		992	978
		Benzene−Water		
300	715	876	1045	997
323	700		1005	987
343	682		944	978
		Chloroform−Water		
300	1476	1483	1062	997
		Octan-1-ol−Water		
300	866	827	1036	997

[a]The corresponding experimental densities are taken from refs 25, 51, and 56.

case of the alcohol molecule, the total density profile is decomposed into the profiles of the apolar (C1) and polar (P1) groups. To better interpret these profiles, we compare in Figure 7e the profiles of these groups in the alkane−water and alcohol−water systems. First, the interfacial region is broader with the alcohol molecule in line with the recent atomistic simulations.[52] Second, the profile of the polar group penetrates further in the water phase than that of the apolar group in line with the atomistic simulations of this system.[52] Interestingly, the mole fraction solubility of water into the octanol-rich phase, calculated from these density profiles is 0.15 ± 0.1 against an experimental value of 0.27[59] and a simulated value (from atomistic simulations[52]) of 0.26. This small solubility of water into the alcohol phase predicted by the MARTINI force field is in line with a too large value of the interfacial tension. The composition of the interfacial region is then correctly reproduced for this degree of coarse-graining although some features such as the network of hydrogen bonds, the alignment of the dipoles cannot be addressed by the degree of coarse-graining of the MARTINI model.

4. CONCLUSIONS

This study reports coarse-grained two-phase simulations of liquid−liquid interfaces of organic−water systems at different temperatures. We have used the MARTINI force field to describe the interactions between the different beads in the systems. We took care to control the methodology of the interfacial tension calculation by using three different definitions and to represent this property through profiles along the normal to the interface. We have checked that some input parameters such as the time step, the simulation time, the system sizes have no effect of the results of the two-phase simulations. It means that the deviations between experiments and simulations cannot be explained by methodological issues but only by the inability of the model to reproduce this interfacial property.

We have focused on different organic−water liquid−liquid interfaces, from the nonpolar alkanes−water and benzene−water systems to a more polar chloroform−water system. The main conclusion is that the current version of the MARTINI force field allows a prediction of the interfacial tension within ±10 mN m^{-1} with respect to experiments, although in some cases the prediction can be better (cyclohexane−water) or poorer (benzene−water).

Concerning the prediction of the interfacial tension of linear alkane−water systems, the MARTINI force field shows deviations from experiments of about 20%. Such deviations have already been observed in the case of atomistic force fields. The decrease of the interfacial tension with the temperature is slightly overestimated compared to experiments. The chloroform−water interface exhibits some deviations between calculated and experimental interfacial tensions. The level of coarse-graining cannot reproduce the specific orientation of the chloroform molecule at the interface. A top-down approach is then required to improve the force field for a better quality prediction of the interfacial tension. Concerning the octanol−water system, the composition of the interfacial region is in line with that provided by molecular simulations with, however, a smaller solubility of the water in the alcohol phase for the CG model. This bad reproduction of the solubility of water is in line with an overestimated interfacial tension.

As already mentioned in the Introduction of this paper, the development of new parameters for the MARTINI force field is outside the scope of this study, but the results presented here allow us to check that this CG force field can be used to simulate liquid−liquid interfaces. We have observed that, when the interfacial region is affected by different specific orientations and associations between the molecules of each phase, the degree of coarse-graining impacts significantly on the description of the interface and, as a consequence, on the value of the interfacial tension. An alternative would consist of doing a new parametrization of the CG force field to better match the interfacial tension. But the need of modeling very well equilibrated liquid−liquid interfaces will help in the future the development of top-down approaches considering the interfacial tension in the experimental database.

APPENDIX A. EXPRESSION OF THE DIFFERENT PARAMETERS FOR THE SHIFTED LENNARD-JONES POTENTIAL

The function $f(r_{iajb}, r_s, r_c)$ of eq 2 is given by the following expression:

$$f(r_{iajb}, r_s, r_c) = -4\epsilon_{ab}\sigma_{ab}^6(r_{iajb} - r_s)^3\left(\frac{1}{3}(\sigma_{ab}^6 A_{12} - A_6) + \frac{1}{4}(r_{iajb} - r_s)(\sigma_{ab}^6 B_{12} - B_6)\right) \quad \text{(A-1)}$$

where the different parameters A_{12}, A_6, B_{12}, and B_6 are expressed as

DOI: 10.1021/acs.jctc.5b00149
J. Chem. Theory Comput. 2015, 11, 3818−3828

$$A_{12} = \frac{12(13r_s - 16r_c)}{r_c^{14}(r_c - r_s)^2}, \quad A_6 = \frac{6(7r_s - 10r_c)}{r_c^{8}(r_c - r_s)^2} \tag{A-2}$$

$$B_{12} = -\frac{12(13r_s - 15r_c)}{r_c^{14}(r_c - r_s)^3}, \quad B_6 = -\frac{6(7r_s - 9r_c)}{r_c^{8}(r_c - r_s)^3} \tag{A-3}$$

The constant C is then defined by

$$C = -4\epsilon_{ab}\sigma_{ab}^6(r_c - r_s)^3\left(\frac{1}{3}(\sigma_{ab}^6 A_{12} - A_6) + \frac{1}{4}(r_c - r_s)(\sigma_{ab}^6 B_{12} - B_6)\right) \tag{A-4}$$

APPENDIX B. EXPRESSION OF THE DIFFERENT PARAMETERS FOR THE SHIFTED ELECTROSTATIC POTENTIAL

For the Coulombic potential, we use $r_s = 0$. The parameters of eq 4 are then expressed as

$$D = -\frac{5}{r_c^4} \qquad E = -\frac{4}{r_c^5} \qquad F = -\frac{2}{3r_c} \tag{B-1}$$

AUTHOR INFORMATION

Corresponding Author

*E-mail: patrice.malfreyt@univ-bpclermont.fr.

Notes

The authors declare no competing financial interest.

REFERENCES

(1) Groot, R. D.; Rabone, K. L. Mesoscopic Simulation of Cell Membrane Damage, Morphology Change and Rupture by Nonionic Surfactants. *Biophys. J.* **2001**, *81*, 725−736.

(2) Ghoufi, A.; Malfreyt, P. Mesoscale Modeling of the Water Liquid-Vapor Interface: A Surface Tension Calculation. *Phys. Rev. E* **2011**, *83*, 051601.

(3) Ghoufi, A.; Malfreyt, P. Coarse Grained Simulations of the Electrolytes at the Water-Air Interface from Many Body Dissipative Particle Dynamics. *J. Chem. Theory Comput.* **2012**, *8*, 787−791.

(4) Spyriouni, T.; Tzoumanekas, C.; Theodorou, D.; Müller-Plathe, F.; Milano, G. Coarse-Grained and Reverse-Mapped United-Atom Simulations of Long-Chain Atactic Polystyrene Melts: Structure, Thermodynamic Properties, Chain Conformation, and Entanglements. *Macromolecules* **2007**, *40*, 3876−3885.

(5) Harmandaris, V. A.; Adhikari, N. P.; van der Vegt, N. F. A.; Kremer, K. Hierarchical Modeling of Polystyrene: From Atomistic to Coarse-Grained Simulations. *Macromolecules* **2006**, *39*, 6708−6719.

(6) Harmandaris, V. A.; Kremer, K. Dynamics of Polystyrene Melts through Hierarchical Multiscale Simulations. *Macromolecules* **2009**, *42*, 791−802.

(7) Mulder, T.; Harmandaris, V. A.; Lyulin, A. V.; van der Vegt, N. F. A.; Kremer, K.; Michels, M. A. J. Structural Properties of Atactic Polystyrene of Different Thermal History Obtained from a Multiscale Simulation. *Macromolecules* **2009**, *42*, 384−391.

(8) Maurel, G.; Schnell, B.; Goujon, F.; Couty, M.; Malfreyt, P. Multiscale Modeling Approach toward the Prediction of Viscoelastic Properties of Polymers. *J. Chem. Theory Comput.* **2012**, *8*, 4570−4579.

(9) Trément, S.; Schnell, B.; Petitjean, L.; Couty, M.; Rousseau, B. Conservative and Dissipative Force Field for Simulation of Coarse-Grained Alkane Molecules: A Bottom-up Approach. *J. Chem. Phys.* **2014**, *140*, 134113.

(10) Lu, L.; Dama, J. F.; Voth, G. A. Fitting Coarse-Grained Distribution Functions Through an Iterative Force-Matching Method. *J. Chem. Phys.* **2013**, *139*, 121906.

(11) Maurel, G.; Schnell, B.; Goujon, F.; Couty, M.; Malfreyt, P. Prediction of Structural and Thermomechanical Properties of Polymers From Multiscale Simulations. *RSC Adv.* **2015**, *5*, 14065−14073.

(12) Maurel, G.; Goujon, F.; Schnell, B.; Malfreyt, P. Multiscale Modeling of the Polymer?Silica Surface Interaction: From Atomistic to Mesoscopic Simulations. *J. Phys. Chem. C* **2015**, *119*, 4817−4826.

(13) Milano, G.; Müller-Plathe, F. Mapping Atomistic Simulations to Mesoscopic Models:? A Systematic Coarse-Graining Procedure for Vinyl Polymer Chains. *J. Phys. Chem. B* **2005**, *109*, 18609−18619.

(14) Carbone, P.; Negri, F.; Müller-Plathe, F. The Conformation of Amine- and Amide-Terminated Poly(Propylene Imine) Dendrimers as Investigated by Molecular Simulation Methods. *Macromolecules* **2007**, *40*, 7044−7055.

(15) Qian, H. J.; Carbone, P.; Chen, X.; Karimi-Varzaneh, H. A.; Liew, C. C.; Müller-Plathe, F. Temperature-Transferable Coarse-Grained Potentials for Ethylbenzene, Polystyrene, and their Mixtures. *Macromolecules* **2008**, *41*, 9919−9929.

(16) Qian, H. J.; Liew, C. C.; Müller-Plathe, F. Effective Control of the Transport Coefficients of a Coarse-Grained Liquid and Polymer Models Using the Dissipative Particle Dynamics and Lowe-Andersen Equations of Motion. *Phys. Chem. Chem. Phys.* **2009**, *11*, 1962−1969.

(17) Carbone, P.; Varzaneh, H.; Müller-Plathe, F. Transferability of Coarse-Grained Force Fields: The Polymer Case. *J. Chem. Phys.* **2008**, *128*, 064904.

(18) Guerrault, X.; Rousseau, B.; Farago, J. Dissipative Particle Dynamics Simulations of Polymer Melts. I. Building Potential of Mean Force for Polyethylene and Cis-Polybutadiene. *J. Chem. Phys.* **2004**, *121*, 6538−6546.

(19) Lahmar, F.; Rousseau, B. Influence of the Adjustable Parameters of the DPD on the Global and Local Dynamics of a Polymer Melt. *Polymer* **2007**, *48*, 3584−3592.

(20) Lahmar, F.; Tzoumanekas, C.; Theodorou, D. N.; Rousseau, B. Onset of Entanglements Revisited. Dynamical Analysis. *Macromolecules* **2009**, *42*, 7485−7494.

(21) Ibergay, C.; Malfreyt, P.; Tildesley, D. J. Electrostatic Interactions in Dissipative Particle Dynamics: Toward a Mesoscale Modeling of the Polyelectrolyte Brushes. *J. Chem. Theory Comput.* **2009**, *5*, 3245−3259.

(22) Ibergay, C.; Malfreyt, P.; Tildesley, D. J. Mesoscale Modeling of Polyelectrolyte Brushes with Salt. *J. Phys. Chem. B* **2010**, *114*, 7274−7285.

(23) Ghoufi, A.; Malfreyt, P.; Emile, J. Recent Advances in Many Body Dissipative Particles Dynamics Simulations of Liquid-Vapor Interfaces. *Eur. Phys. J. E: Soft Matter Biol. Phys.* **2013**, *36*, 10.

(24) Marrink, S. J.; de Vries, A. H.; Mark, A. E. Coarse Grained Model for Semiquantitative Lipid Simulations. *J. Phys. Chem. B* **2004**, *108*, 750−760.

(25) Marrink, S. J.; Risselada, H. J.; Yefimov, S.; Tieleman, D. P.; de Vries, A. H. The MARTINI Force Field: Coarse Grained Model for Biomolecular Simulations. *J. Phys. Chem. B* **2007**, *111*, 7812−7824.

(26) Monticelli, L.; Kandasamy, S. K.; Periole, X.; Larson, R. G.; Tieleman, D. P.; Marrink, S. J. The MARTINI Coarse-Grained Force Field: Extension to Proteins. *J. Chem. Theory Comput.* **2008**, *4*, 819−834.

(27) Lopez, C. A.; Rzepiela, A. J.; de Vries, A. H.; Dijkhuizen, L.; Hünenberger, P. H.; Marrink, S. J. Martini Coarse-Grained Force Field: Extension to Carbohydrates. *J. Chem. Theory Comput.* **2009**, *5*, 3195−3210.

(28) Yesylevskyy, S. O.; Schäfer, L. V.; Sengupta, D.; Marrink, S. J. Polarizable Water Model for the Coarse-Grained MARTINI Force Field. *PLoS Comput. Biol.* **2010**, *6*, e1000810.

(29) Sergi, D.; Scocchi, G.; Ortona, A. Coarse-graining MARTINI Model for Molecular-Dynamics Simulations of the Wetting Properties of Graphitic Surfaces with Non-Ionic, Long-Chain, and T-Shaped Surfactants. *J. Chem. Phys.* **2012**, *137*, 094904.

(30) Marrink, S. J.; Tieleman, D. P. Perspective on the Martini model. *Chem. Soc. Rev.* **2013**, *42*, 6801−6822.

DOI: 10.1021/acs.jctc.5b00149
J. Chem. Theory Comput. 2015, 11, 3818−3828

(31) Darden, T.; York, D.; Pedersen, L. Particle Mesh Ewald: an N log(N) Method for Ewald Sums in Large Systems. *J. Chem. Phys.* **1993**, *98*, 10089−10092.
(32) de Jong, D. H.; Singh, G.; Bennett, W. F. D.; Arnarez, C.; Wassenaar, T. A.; Schäfer, L. V.; Periole, X.; Tieleman, D. P.; Marrink, S. J. Improved Parameters for the Martini Coarse-Grained Protein Force Field. *J. Chem. Theory Comput.* **2013**, *9*, 687−697.
(33) Irving, J. H.; Kirkwood, J. G. The Statistical Mechanical Theory of Transport Processes. IV. The Equations of Hydrodynamics. *J. Chem. Phys.* **1950**, *18*, 817−829.
(34) Rowlinson, J. S.; Widom, B. *Molecular Theory of Capillarity*; Clarendon Press: Oxford, 1982.
(35) Walton, J. P. R. B.; Tildesley, D. J.; Rowlinson, J. S.; Henderson, J. R. The pressure Tensor at the Planar Surface of a Liquid. *Mol. Phys.* **1983**, *48*, 1357−1368.
(36) Walton, J. P. R. B.; Gubbins, K. E. The Pressure Tensor in an Inhomogeneous Fluid of Non-Spherical Molecules. *Mol. Phys.* **1985**, *55*, 679−688.
(37) Neyt, J. C.; Wender, A.; Lachet, V.; Ghoufi, A.; Malfreyt, P. Quantitative Predictions of the Interfacial Tensions of Liquid-Liquid Interfaces through Atomistic and Coarse Grained Models. *J. Chem. Theory Comput.* **2014**, *10*, 1887−1899.
(38) Gloor, G. J.; Jackson, G.; Blas, F. J.; de Miguel, E. Test-Area Simulation Method for the Direct Determination of the Interfacial Tension of Systems with Continuous or Discontinuous Potentials. *J. Chem. Phys.* **2005**, *123*, 134703.
(39) Ghoufi, A.; Goujon, F.; Lachet, V.; Malfreyt, P. Expressions for Local Contributions to the Surface Tension from the Virial Route. *Phys. Rev. E* **2008**, *77*, 031601.
(40) Martínez, L.; Andrade, R.; Birgin, E. G.; Martínez, J. M. Packmol: A Package for Building Initial Configurations for Molecular Dynamics Simulations. *J. Comput. Chem.* **2009**, *30*, 2157−2164.
(41) DL_POLY is a parallel molecular dynamics simulation package developed at the Daresbury Laboratory Project for Computer Simulations under the auspices of the EPSRC for the Collaborative Computational Project for Computer Simulation of Condensed Phases (CCP5) and the Advanced Research Computing Group (ARCG) at the Daresbury Laboratory.
(42) Todorov, I. T.; Smith, W.; Trachenko, K.; Dove, M. T. DL_POLY_3: New Dimensions in Molecular Dynamics Simulations via Massive Parallelism. *J. Mater. Chem.* **2006**, *16*, 1911−1918.
(43) Berendsen, H. J. C.; Postma, J. P. M.; van Gunsteren, W.; DiNola, A.; Haak, J. R. Molecular-Dynamics with Coupling to an External Bath. *J. Chem. Phys.* **1984**, *81*, 3684−3690.
(44) Ibergay, C.; Ghoufi, A.; Goujon, F.; Ungerer, P.; Boutin, A.; Rousseau, B.; Malfreyt, P. Molecular Simulations of the n-Alkane Liquid-Vapor Interface: Interfacial Properties and their Long Range Corrections. *Phys. Rev. E* **2007**, *75*, 051602.
(45) Baoukina, S.; Marrink, S. J.; Tieleman, D. P. Lateral Pressure Profiles in Lipid Monolayers. *Faraday Discuss.* **2010**, *144*, 393−409.
(46) Winger, M.; Trzesniak, D.; Baron, R.; van Gunsteren, W. F. On Using a too Large Integration Time Step in Molecular Dynamics Simulations of Coarse-Grained Molecular Models. *Phys. Chem. Chem. Phys.* **2009**, *11*, 1934−1941.
(47) Marrink, S.; Periole, X.; Tieleman, D. P.; de Vries, A. H. Comment on "On using a too large Integration Time Step in Molecular Dynamics Simulations of Coarse-Grained Molecular Models" by M. Winger, D. Trzesniak, R. Baron and W. F. van Gunsteren. *Phys. Chem. Chem. Phys.* **2009**, *11*, 1934; *Phys. Chem. Chem. Phys.* **2010**, *12*, 2254−2256.
(48) van Gunsteren, W. F.; Winger, M. Reply to the 'Comment on "On Using a Too Large Integration Time Step in Molecular Dynamics Simulations of Coarse-Grained Molecular Models"' by S. J. Marrink, X. Periole, D. Peter Tieleman and Alex H. de Vries. *Phys. Chem. Chem. Phys.* **2010**, *12*, 2257−2258; *Phys. Chem. Chem. Phys.* **2010**, *12*, 2257−2258.
(49) Alpbaz, M.; Tutkun, B. O.; Bilgesu, A. The Measurement of Interfacial Tension by Drop Weight Method. *Commun. Fac. Sci. Univ. Ankara, Ser. B: Chem. Chem. Eng.* **1988**, *34*, 103−112.
(50) Zeppieri, S.; Rodriguez, J.; Lopez de Ramos, A. L. Interfacial Tension of Alkane + Water Systems. *J. Chem. Eng. Data* **2001**, *46*, 1086−1088.
(51) Ghate, M. H.; Ghazipour, H. Highly Accurate Liquid-Liquid Interfacial Tension Measurement by a Convenient Capillary Apparatus. *Fluid Phase Equilib.* **2014**, *377*, 76−81.
(52) Wick, C. D.; Chang, T. M. Computational Observation of Pockets of Enhanced Water Concentration at the 1-Octanol/Water Interface. *J. Phys. Chem. B* **2014**, *118*, 7785−7791.
(53) Mayoral, E.; Goicochea, A. G. Modeling the Temperature Dependent Interfacial Tension between Organic Solvents and Water using Dissipative Particle Dynamics. *J. Chem. Phys.* **2013**, *138*, 094703.
(54) Zhang, Y.; Feller, S. E.; Brooks, B. R.; Pastor, R. W. Computer Simulation of Liquid/Liquid Interfaces. I. Theory and Application to Octane/Water. *J. Chem. Phys.* **1995**, *103*, 10252−10266.
(55) Nickerson, S.; Frost, D. S.; Phelan, H.; Dai, L. L. Comparison of the Capillary Wave Method and Pressure Tensor Route for Calculation of Interfacial Tension in Molecular Dynamics Simulations. *J. Comput. Chem.* **2013**, *34*, 2707−2715.
(56) Demond, A. H.; Lindner, A. S. Estimation of Interfacial Tension between Organic Liquids and Water. *Environ. Sci. Technol.* **1993**, *27*, 2318−2331.
(57) Hore, D. K.; Walker, D. S.; MacKinnon, L.; Richmond, G. L. Molecular Structure of the Chloroform-Water and Dichloromethane-Water Interfaces. *J. Phys. Chem. C* **2007**, *111*, 8832−8842.
(58) Mcfearin, C.; Richmond, G. L. The Unique Molecular Behavior of Water at the Chloroform-Water Interface. *Appl. Spectrosc.* **2010**, *64*, 986−994.
(59) Lang, B. E. Solubility of Water in Octan-1-ol from (275 to 369) K. *J. Chem. Eng. Data* **2012**, *57*, 2221−2226.

DOI: 10.1021/acs.jctc.5b00149
J. Chem. Theory Comput. 2015, 11, 3818−3828